

Supplementary methods:

Materials. Palmitate (PA) (P0500) was obtained from Sigma-Aldrich (St. Louis, MO). AGI-1067 (216167-82-7) was from MedChemExpress (Princeton, NJ). URM-099 was kindly provided by Dr. Harris A. Gelbard (University of Rochester Medical Center, Rochester, NY). Alpha-Tocopherol (258024) was purchased from Sigma-Aldrich. SB203580 (559389) was from Millipore Sigma (St. Louis, MO, USA). Primary antisera employed for the studies include: anti-alpha smooth muscle actin (α -SMA) (ab124964) from Abcam (Cambridge, MA), anti-p-p38 (9211), anti-p38 (9212), anti-p-MKK3/MKK6 (12280), anti-MKK3 (8535), p-JNK (9255), JNK (9252), anti-F4/80 (70076), anti-human VCAM-1 (13662), and anti-mouse VCAM-1 (32653) from Cell Signaling Technology (Danvers, MA), anti-GAPDH (MAB374) from Millipore Sigma, anti- β -actin (sc-47778) from Santa Cruz Biotechnologies (Santa Cruz, CA), and anti-galectin-3 (14530181) from Thermo Fisher Scientific (Waltham, MA). Neutralizing anti-VCAM-1 antibody (GTX14360) and IgG isotype control (BE0088) were obtained from GeneTex and InVivoMab, respectively.

Cells. Primary human liver sinusoidal endothelial cells (LSEC) were purchased from ScienCell Research Laboratories (San Diego, CA). To harvest primary mouse LSECs, cell suspensions were obtained using the liver collagenase perfusion method as

previously described by us (1), and centrifuged at 50g for 2 minutes to remove hepatocytes. The supernatant which includes non-parenchymal cells was subjected to LSEC isolation using CD146 MicroBeads (Miltenyi Biotec, Bergisch Gladbach, Germany) following the manufacture's instruction. TSEC, primary human LSEC, and primary mouse LSEC were cultured in Endothelial Cell Growth Medium (ECM, ScienCell Research Laboratories) consisting of 5% fetal bovine serum (FBS), 1% endothelial cells growth supplement, and 1% primocin (InVivoGen, San Diego, CA) solution. All the cell cultures were maintained at 37°C in a humidified atmosphere of 5% CO₂.

PA treatment of cells. PA was dissolved in isopropanol at a concentration of 80 mM as a stock solution.(2) The PA stock solution was added to Endothelial Cell Growth Medium containing 1% fatty acid free low endotoxin bovine serum albumin (BSA); the final experimental concentrations of PA 250 or 500 μM were used for the treatment of cells. For the negative control non-treated (vehicle-treated) cells, the same concentration of isopropanol was added to Endothelial Cell Growth Medium containing 1% BSA.

Cell viability assay To evaluate cytotoxicity, human LSEC were plated in 96-well plates (5×10^4 cells per well), cultured overnight, and then treated with vehicle or 500 μM of PA for 16 hours. Cell viability was evaluated using Cell Titer-Glo luminescent assay

according to the manufacturer's instructions (Promega, Madison, WI, USA).

Immunoblot analysis. Cells were lysed using RIPA buffer (50 mM Tris-HCl, pH 7.4; 1% Nonidet P-40; 0.25% sodium deoxycholate; 150 mM NaCl; 1 mM EDTA with protease inhibitors) followed by centrifugation at 15,000g for 15 min at 4°C. Protein concentrations of the lysates were measured by the Bradford assay method (Sigma-Aldrich). Equal amount of protein were loaded onto Sodium dodecyl sulfate (SDS)-Polyacrylamide gel electrophoresis (PAGE) gels, transferred to nitrocellulose membrane (Bio-Rad, Hercules, CA) and incubated overnight with the primary antibody of interest. All primary antibodies were used at a dilution of 1:1,000 unless otherwise recommended by the manufacturer. Horseradish peroxidase-conjugated secondary antibodies against rabbit (Alpha Diagnostic International, San Antonio, TX) or mouse (Southern Biotech, Birmingham, AL) were used at a dilution of 1:5,000 and incubated for 1 hour at room temperature. Proteins were detected using enhanced chemiluminescence reagents (GE Healthcare, Chicago, IL). β -actin and GAPDH protein levels were used as loading controls. Densitometry analysis of the blots was performed using ImageJ software (National Institutes of Health, Bethesda, MD, USA).

Animals. Study protocols were conducted as approved by the Institutional Animal Care and Use Committee (IACUC) of Mayo Clinic. The methods employed in the current

study were conducted in accordance with IACUC guidelines for the use of anesthetics in experimental mice. Mice were housed and bred in a temperature-controlled 12:12-hour light-dark cycle facility with free access to diet. All interventions occurred during the light cycle. C57BL/6J mice were purchased from Jackson Laboratory (Bar Harbor, ME). *Mlk3^{-/-}* mice were gifted by Dr. Davis.(3, 4)

Diet-induced murine NASH studies: C57BL/6J wild-type (WT) mice and *Mlk3^{-/-}* mice were fed either a chow diet (5053 PicoLab Rodent Diet 20, LabDiet, St Louis, MO) or a diet rich in fat, fructose, and cholesterol (FFC) starting at the age of 8-weeks for 24 weeks. FFC diet consists of 40% energy as fat (12% saturated fatty acid, 0.2% cholesterol) (AIN-76A Western Diet, TestDiet, St Louis, MO), with fructose (23.1 g/L) and glucose (18.9 g/L) in the drinking water. The FFC diet induces steatohepatitis with pronounced hepatocellular ballooning, lipoapoptosis, and progressive fibrosis with a high fidelity to the human NASH histology and metabolic profile, (5) and have been well validated by us.(3, 6) At 20 weeks on the diet, the mice were randomized to receive either anti-VCAM-1 neutralizing antibody (M/K-2.7), (Genetex, GTX14360) or IgG isotype antibody (BE0088, InVivoMAb). Mice were injected with 10 mg/kg body weight of either the antibodies or IgG isotype intraperitoneally, twice per week for the last 4 weeks of the feeding studies. In a separate study, chow and FFC diet-fed mice were randomized

to receive either vehicle or the VCAM-1 inhibitor succinobucol (AGI-1067). Mice were injected with either vehicle or 25 mg/kg body weight of AGI-1067 intraperitoneally, daily for the last 15 days of the feeding study. In an independent study, *Vcam1*^{fl/fl} and *Vcam1*^{Δend} mice were fed the choline-deficient high-fat diet (CD-HFD) (Research Diet, Cat. A06071302), which consists of 60% fat, 0.1% methionine, and no added choline, starting at 8 weeks of age for 6 weeks. Mice fed the CD-HFD experienced minimal body weight loss compared to the traditional choline-deficient diet. (7) Moreover, the CD-HFD induces hepatic steatosis, ALT elevation, hepatocytes ballooning, hepatic inflammation and fibrosis, recapitulating the histological features of human NASH in a short period of time.(7, 8)

Assessment of metabolic profiles in mice. Total caloric intake at the 3rd week of VCAM-1 antibody treatment and the first week of AGI-1067 treatment was calculated based on the weight of food and drinking water consumption. At the third week of anti-VCAM-1 neutralizing antibody treatment, metabolic parameters, including oxygen consumption, carbon dioxide production, and locomotor activity, were measured using a Comprehensive Lab Animal Monitoring System (CLAMS, Columbus Instruments, OH), as previously described.(9) Anti-VCAM-1 antibody from Bio Xcell (West Lebanon, NH), (BE0027) was used for the CLAMS study. Blood glucose levels and plasma insulin

levels were measured using Assure 4 (Arkray, Edina, MN) and Ultra-Sensitive Mouse Insulin enzyme-linked immunosorbent assay (ELISA) kit (Crystal Chem Inc., Downers Grove, IL), respectively. Homeostasis model assessment of insulin resistance (HOMA-IR) was calculated by using the following formula: $\text{HOMA-IR} = 26 \times \text{fasting insulin level (ng/mL)} \times \text{fasting glucose level (mg/dL)} / 405$. (10) Mice were sacrificed under general anesthesia induced by a ketamine/xylazine cocktail (83 mg/kg ketamine, 16 mg/kg xylazine, intraperitoneal injection). Blood and liver samples were collected for further studies. Glucose tolerance test (GTT) was performed at 23 weeks of the feeding study by serial measurement of blood glucose at fasting status and then at 15, 30, 60, and 120 minutes after intraperitoneal administration of a glucose bolus of 1.5 g/kg.

Liver triglyceride and alanine aminotransferase measurement. Liver triglyceride levels were measured in mouse liver homogenates. Fifty milligrams of liver tissue was homogenized in a 5% NP-40 solution. EnzyChrom Triglyceride Kit (BioAssay System, CA) was used for the assay according to the manufacturer's instruction. Photometric absorbance was read at 570 nm using a Synergy H1 microplate reader (BioTek). Serum alanine aminotransferase (ALT) levels were measured by VetScan2 (Abaxis Veterinary Diagnostics, Union City, CA).

Histology, immunohistochemistry, and digital image analysis. Liver histology was

performed using tissue fixed in 10% formalin, dehydrated, and embedded in paraffin. Hematoxylin and eosin (H&E) staining and Sirius red staining were performed as described previously.(11) Severity of NASH was assessed using nonalcoholic fatty liver disease (NAFLD) activity score (NAS), a semi-quantitative score that accounts for steatosis, ballooned hepatocytes, and lobular inflammation.(12) The NAS score was assessed in 10 random fields per slide per animal, and the mean value was used as the NAS score for each animal. Terminal deoxynucleotidyl transferase deoxyuridine triphosphate nick-end labeling (TUNEL) assay was performed using the *In Situ* Cell Death Detection Kit (Roche) following manufacturer's instruction. For the immunohistochemistry studies, formalin-fixed paraffin-embedded liver tissue sections were deparaffinized, hydrated, and stained with antibody against VCAM-1 (1:200), F4/80 (1:500), galectin-3 (1:250) or alpha smooth muscle actin (α -SMA) (1:1000) for mouse tissues, and VCAM-1 (1:500) for human tissues. Bound antibodies derived from mouse or rabbit were detected using a Vectastain ABC kit (Vector Laboratories) or EnVision System HRP (Dako), respectively, and DAB substrate (Vector Laboratories) according to the manufacturer's instructions; the tissue sections were counterstained with hematoxylin. Sirius red-positive, VCAM-1, F4/80, galectin-3 or α -SMA-positive areas were quantified by digital image analysis of 10 random fields per slide per animal using

the ImageJ software. TUNEL-positive cells were quantified by counting positive nuclei in 10 random fields per slide per animal.

Quantitative real-time PCR. Total RNA was isolated with the RNeasy Mini Kit (Qiagen, Valencia, CA) and was reverse transcribed with moloney murine leukemia virus reverse transcriptase and oligo-dT random primers (both from Invitrogen, CA, USA). Quantification of gene expression was performed by real-time PCR using SYBR green fluorescence on a LightCycler 480 instrument (Roche Applied, IN, USA) (Primers are listed in Supplementary Table 6). Target gene expression was calculated using the $\Delta\Delta C_t$ method and was normalized to *18S* rRNA expression levels, which were stable across experimental groups.

Supplementary Table 1

List of previously reported endothelial cells “candidate genes” involved in leukocyte adhesion

Gene Name	Coding Protein	logFC	logCPM	P-value	FDR
<i>Icam1</i>	Icam-1	1.99673	4.16670	3.31E-39	1.55E-37
<i>Vcam1</i>	Vcam-1	1.93006	4.75147	2.51E-36	9.32E-35
<i>Cd34</i>	Cd34	1.18150	1.65911	0.01070	0.01656
<i>Jam2</i>	Jam2	0.50787	3.70723	0.07195	0.09705
<i>Jam3</i>	Jam3	-0.03984	0.49045	0.86940	0.89454
<i>Sdc1</i>	syndecan 1	-0.21166	7.83332	0.26668	0.31932
<i>Esam</i>	Esam	-0.44312	3.52181	0.00033	0.00064
<i>Icam2</i>	Icam-2	-0.49807	1.87062	0.00480	0.00785
<i>Cd99l2</i>	CD99 antigen-like 2	-0.56098	5.00962	2.67E-08	0.00000
<i>Selp</i>	P-selectin	-1.18820	2.88897	9.37E-14	5.11E-13
<i>Sdc4</i>	syndecan 4	-1.40948	8.41017	4.77E-25	6.95E-24
<i>Madcam1</i>	Madcam-1	ND	ND	ND	ND
<i>Sele</i>	E-selectin	ND	ND	ND	ND
<i>Aoc3</i>	VAP-1	ND	ND	ND	ND

logFC: log₂ fold change; logCPM: log counts per million reads; FDR: false-discovery rate; ND: not detected; Icam: intercellular adhesion molecule; Madcam: mucosal addressin cell adhesion molecule; Jam: junctional adhesion molecule; Esam: endothelial cell-selective adhesion molecule; VAP: vascular adhesion protein

Supplementary Table 2

Top 90 open chromatin regions (OCRs) located in promoter regions differentially abundant in LSEC derived from FFC-fed mice detected by assay for transposase-accessible chromatin by sequencing (ATAC-seq)

Chr	Start	End	Conc. Chow	Conc. FFC	Log FC	p-value	Corresponding Gene
chr1	40084565	40084716	1.14	3.85	2.72	0.000128	Il1r2
chr2	173218686	173218994	1.73	4.22	2.49	9.08E-05	Zbp1
chr11	6292473	6292651	1.56	3.84	2.28	0.00114	Ogdh
chr2	79254831	79254939	1.66	3.76	2.1	0.00106	Itga4
chr11	80089379	80089515	1.24	3.33	2.09	0.00443	Atad5
chr11	120948953	120949099	2.09	4.11	2.02	0.000242	Slc16a3
chr8	27175142	27175286	1.64	3.64	2	0.00197	Rab11fip1
chr11	69666126	69666291	2.14	4.11	1.97	0.000863	Cd68
chr1	152807687	152807863	1.94	3.9	1.95	0.00183	Ncf2
chr17	34287791	34287991	2.5	4.39	1.9	0.00014	H2-Aa
chr14	26534391	26534536	1.66	3.55	1.89	0.00535	Slmap
chr10	128909633	128909974	3.11	4.94	1.83	8.70E-05	Cd63
chr7	127091225	127091377	1.95	3.76	1.81	0.00331	AI467606
chr11	54962914	54963085	2.7	4.4	1.7	0.000868	Tnip1
chr9	92250091	92250328	2.49	4.15	1.66	0.00236	Plscr1
chr1	164115106	164115358	2.34	3.94	1.6	0.00579	Selp
chr12	88953016	88953362	2.95	4.53	1.59	0.00114	Nrxn3
chr8	88636057	88636210	2.42	3.99	1.57	0.00993	Snx20
chr5	137030120	137030325	2.67	4.24	1.56	0.00354	Vgf
chr5	92328019	92328321	3.23	4.77	1.53	0.00128	Cxcl9
chr5	110387026	110387241	2.17	3.7	1.53	0.00892	Fbrsl1
chr7	110862721	110863302	4.33	5.79	1.46	9.21E-05	Lyve1
chr3	10208493	10208722	2.7	4.14	1.44	0.00475	Fabp4
chr4	119108547	119109016	4.26	5.62	1.36	0.00037	Slc2a1
chr1	131152983	131153263	3.28	4.64	1.36	0.00351	Eif2d
chr19	37376017	37376532	4.68	6.03	1.35	0.000108	Kif11
chr1	194938751	194938981	2.97	4.32	1.34	0.00506	Cd34
chr7	38183157	38183332	2.75	4.1	1.34	0.0084	1600014C10Rik

Supplementary Table 2 (continued)

Chr	Start	End	Conc. Chow	Conc. FFC	Log FC	p-value	Corresponding Gene
chr17	35242708	35242874	2.95	4.27	1.32	0.00927	Ddx39b
chr13	42301322	42301653	3.31	4.62	1.31	0.00462	Edn1
chr2	165055335	165055752	3.87	5.16	1.3	0.0033	Cd40
chr14	30923337	30923717	3.56	4.85	1.29	0.00342	Itih3
chr17	33919433	33919628	3.26	4.55	1.29	0.0081	Tapbp
chr17	86962407	86962666	3.73	5.01	1.27	0.00305	Rhoq
chr5	17835707	17836167	3.43	4.7	1.27	0.00738	Cd36
chr3	116129326	116129793	3.44	4.71	1.26	0.0052	Vcam1
chr17	34263100	34263385	3.23	4.49	1.26	0.00637	H2-Ab1
chr10	63386494	63386760	3.22	4.48	1.26	0.00699	Dnajc12
chrX	137049392	137049744	3.7	4.95	1.25	0.00535	Fam199x
chr4	152185602	152185840	2.97	4.21	1.25	0.00959	Acot7
chr15	76246663	76246980	3.79	5.03	1.24	0.00354	Grina
chr11	120823931	120824892	5.75	6.97	1.22	0.00111	Fasn
chr11	70982800	70983168	4.27	5.5	1.22	0.00202	C1qbp
chrX	8132427	8132905	3.55	4.77	1.22	0.00671	Wdr13
chr6	116673794	116674083	3.21	4.43	1.22	0.00852	Rassf4
chr11	109473597	109474084	4.54	5.75	1.21	0.00142	Slc16a6
chr15	25843067	25843509	3.61	4.82	1.21	0.0045	Retreg1
chr10	75893077	75893484	3.92	5.11	1.2	0.00318	Derl3
chr15	76656895	76657159	3.89	5.09	1.19	0.0033	Cyhr1
chr11	60210344	60210722	4.51	5.7	1.19	0.00399	Srebf1
chr7	41393141	41393662	4.62	5.81	1.19	0.00501	AI987944
chr7	30422082	30422458	4.25	5.44	1.18	0.0015	Nfkbid
chr9	7872622	7873237	5.61	6.79	1.18	0.00384	Birc3
chr7	135605198	135605631	3.67	4.86	1.18	0.00621	Ptpre
chr11	68431773	68432229	4.03	5.21	1.17	0.00283	Pik3r5
chr10	13090547	13090995	4.01	5.17	1.17	0.00383	Plagl1
chr8	122576713	122576995	3.23	4.41	1.17	0.00842	Aprt
chr8	110846657	110847139	3.85	5.01	1.16	0.00802	Sf3b3
chr19	6992490	6992808	4.61	5.76	1.15	0.00272	Dnajc4

Supplementary Table 2 (continued)

Chr	Start	End	Conc. Chow	Conc. FFC	Log FC	p-value	Corresponding Gene
chr15	79348085	79348482	4.71	5.86	1.15	0.0051	Maff
chr12	104262857	104263242	4.48	5.63	1.15	0.00974	Serpina3i
chr13	22035550	22035899	3.98	5.12	1.14	0.00323	Hist1h2ah
chr19	44293652	44294095	4.34	5.49	1.14	0.00329	Scd2
chr17	56613261	56613596	4.21	5.35	1.14	0.00553	Rpl36
chr8	106337770	106338315	5.28	6.41	1.13	0.00633	Smpd3
chr12	112678641	112678956	4.07	5.2	1.13	0.00682	Zbtb42
chr15	99029840	99030435	4.5	5.61	1.11	0.00325	Tuba1c
chr5	115134801	115135087	3.66	4.77	1.11	0.00671	Unc119b
chr11	115933442	115933785	4.5	5.6	1.1	0.00387	Sap30bp
chr16	30388581	30388952	3.75	4.85	1.1	0.00645	Atp13a3
chr1	39577097	39577641	4.73	5.81	1.09	0.00272	Rnf149
chr2	30828181	30828528	4.45	5.54	1.09	0.00895	Asb6
chr11	60811090	60811456	4.48	5.54	1.07	0.00719	Shmt1
chr19	5118183	5118506	4.08	5.16	1.07	0.00878	Klc2
chr7	96951275	96951947	5.34	6.4	1.06	0.00642	Nars2
chr5	113772595	113772963	4.54	5.6	1.06	0.00675	Iscu
chr6	124662524	124663273	6.21	7.27	1.06	0.00801	Lpcat3
chr11	99024102	99024515	4.48	5.53	1.05	0.00833	Top2a
chr11	95413762	95414304	5.29	6.33	1.04	0.00466	Spop
chr9	57439974	57440253	4.01	5.05	1.04	0.007	Ppcdc
chr11	109473069	109473535	4.48	5.52	1.04	0.00703	Arsg
chr5	138279941	138280408	4.26	5.3	1.04	0.00751	Gpc2
chr10	80016488	80016919	4.55	5.57	1.03	0.00339	Arhgap45
chr7	100863053	100863640	5.17	6.18	1.02	0.00352	Relt
chr2	127335817	127336447	4.98	6	1.02	0.00819	Dusp2
chr7	45434225	45434950	6.26	7.28	1.02	0.00912	Ruvbl2
chr19	36925757	36926482	5.8	6.83	1.02	0.00962	Btaf1
chr19	34192176	34192822	4.66	5.67	1.01	0.00572	Stambpl1
chr11	88999165	88999656	5.05	6.06	1.01	0.00881	Trim25

chr: chromosome; start/end: base pair numbers of start/end sites of OCRs on the chromosome; conc.: concentration; logFC: log fold change

Supplementary Table 3**Top 53 transcripts differentially expressed by RNA-sequencing in LSEC derived from FFC-fed mice**

GeneName	p-value	log ₂ FC
GpnmB	1.13E-80	8.1478
Mmp12	6.13E-70	6.5183
Ccl9	3.78E-55	4.7002
Atp6v0d2	4.48E-45	6.9286
Ms4a4a	3.65E-40	4.6438
Trem2	1.84E-39	4.9426
Il1rn	4.59E-39	3.3878
Slc7a11	8.12E-38	4.3800
Clec5a	2.36E-37	3.5730
Gdf3	6.92E-36	5.9659
Mmp13	1.56E-35	4.1112
Cx3cr1	8.59E-35	3.6983
Ccr2	2.90E-32	3.2980
Ccl2	6.24E-29	2.6967
Ptafr	1.30E-28	3.2874
Siglecf	4.96E-26	3.3198
Itgax	9.88E-25	3.5323
Ctsj	2.11E-24	6.4864
Il1f9	2.43E-24	2.7849
Apoa4	3.97E-24	3.5917
Olr1	6.43E-24	3.2995
Armcx4	7.68E-24	2.0793
Gpr34	9.01E-24	4.1762
AI427809	4.63E-23	4.0279
Chil3	6.36E-23	4.0122
H2-M2	8.66E-23	4.2333
Plxdc2	4.17E-22	4.0242
Myo5a	8.51E-22	3.3926
Ccrn4l	1.80E-21	2.1723
Obsl1	2.27E-21	2.0495
Gcnt1	7.14E-21	2.8714

Supplementary Table 3 (continued)

GeneName	p-value	log ₂ FC
Clec4e	9.71E-21	3.1870
Atp8b4	1.29E-20	2.9156
Abca1	2.52E-20	1.8075
Ptgs2	2.74E-20	2.7569
4930430E12Rik	3.46E-20	4.6778
Cd63	4.52E-20	2.1215
Gla	6.52E-20	1.5445
Gadd45b	1.78E-19	2.5979
Dpep2	2.07E-19	4.6426
Timp1	3.66E-19	3.0242
Bcl2a1d	1.15E-18	3.0451
Gpr35	1.44E-18	2.3218
Asprv1	2.48E-18	2.4208
Cblb	3.04E-18	1.0265
Vcam1	3.55E-18	0.9258
2010002M12Rik	3.72E-18	3.3500
Sh3pxd2b	3.75E-18	3.3182
Rgs5	3.94E-18	2.4692
Lpl	5.30E-18	2.9186
Clec4d	5.58E-18	2.3549
Pparg	6.44E-18	1.5592
Lat2	8.61E-18	2.8165

Supplementary Table 4**Patients' characteristics in each category based on liver histology.**

	Age (years)	Gender (M/W)	BMI (kg/m ²)	AST (U/L)	ALT (U/L)	Mode of tissue acquisition
Normal Liver	57	M	31.8	15	17	HR
	56	M	34.9	38	21	HR
	69	M	34.2	8	N.D.	HR
	38	F	34.9	28	24	HR
	55	F	45.4	51	24	HR
	78	F	30.7	18	23	HR
Isolated Steatosis	47	M	40.6	72	23	HR
	46	M	45.6	39	19	HR
	29	F	46.5	N.D.	13	HR
	56	F	50.7	23	98	HR
	48	F	42.9	16	15	HR
	63	F	39.5	29	22	HR
	40	M	44.8	N.D.	47	HR
NASH F0-1	49	F	52.1	N.D.	23	HR
	60	F	37.8	11	28	HR
	36	M	39.1	68	39	HR
	45	M	31.3	30	24	HR
	52	M	38.2	127	56	HR
	27	F	40.6	13	13	HR
	26	M	63.2	63	40	HR
NASH F2-4	44	M	45.0	67	55	LB
	58	M	21.0	22	86	HR
	63	F	62.0	44	21	HR
	67	F	45.8	78	83	LB
	56	F	40.3	20	21	HR

HR: hepatic resection; LB: liver biopsy

Supplementary Table 5**CyTOF panel**

	Label	Target	Clone	Volume used (µL)	Supplier/ Catalogue number	
1	089Y	CD45	30-F11	0.5	Fluidigm	3089005B
2	106Cd	CD146	ME-9F1	1	BioLegend	134701
3	141Pr	Lgals3	202213	1	R&D Systems	MAB1197
4	142Nd	CD11c	N418	0.5	Fluidigm	3142003B
5	143Nd	TCRb	H57-597	0.25	Fluidigm	3143010B
6	144Nd	MHC Class I	28-14-8	0.25	Fluidigm	3144016B
7	145Nd	CLEC2	17D9	1	BioLegend	146102
8	147Sm	CD9	MZ3	1	BioLegend	124802
9	149Sm	Tim4	370901	1	BioLegend	130002
10	151Eu	CD206 (MMR)	C068C2	1	BioLegend	141702
11	152Sm	CD3e	145-2C11	0.25	Fluidigm	3152004B
12	153Eu	CLEC4F	poly Goat	1	R&D Systems	AF2784
13	154Sm	CD62L (L-selectin)	MEL-14	1	BioLegend	104402
14	155Gd	MERTK	108928	1	R&D Systems	108928
15	156Gd	CCR2	475301	0.5	R&D Systems	475301
16	159Tb	F4/80	BM8	0.5	Fluidigm	BM8
17	160Gd	CD64	290322	1	R&D Systems	290322
18	161Dy	Ly6G	1A8	0.25	BioLegend	1A8
19	164Dy	CX3CR1	SA011F11	0.25	Fluidigm	SA011F11
20	165Ho	CD14	Sa14-2	1	BioLegend	Sa14-2
21	166Er	CD19	6D5	0.5	Fluidigm	6D5
22	167Er	TREM2	237920	1	R&D Systems	MAB17291
23	168Er	CD8a	53-6.7	0.25	Fluidigm	3168003B
24	169Tm	CD163	S15049I	1	BioLegend	155302
25	170Er	CD161 (NK1.1)	PK136	0.5	Fluidigm	3170002B
26	172Yb	CD11b (Mac-1)	M1/70	0.25	Fluidigm	3172012B
27	174Yb	CD115/CSF1R	AFS98	0.5	BioLegend	135521
28	175Lu	Ly6C	HK1.4	0.25	BioLegend	128039
29	176Yb	CD45R (B220)	RA3-6B2	0.5	Fluidigm	3176002B
30	209Bi	I-A/I-E	M5/114.15.2	0.1	BioLegend	107637

Supplementary Table 6**PCR primers**

Name	Sequence
Mouse <i>Cd68</i> Forward Primer	TGTCTGATCTTGCTAGGACCG
Mouse <i>Cd68</i> Reverse Primer	GAGAGTAACGGCCTTTTTGTGA
Mouse <i>Ccr2</i> Forward Primer	ATCCACGGCATACTATCAACATC
Mouse <i>Ccr2</i> Reverse Primer	CAAGGCTCACCATCATCGTAG
Mouse <i>Tnf-α</i> Forward Primer	CCCTCACACTCAGATCATCTTCT
Mouse <i>Tnf-α</i> Reverse Primer	GCTACGACGTGGGCTACAG
<i>18S</i> Forward Primer	CGCTTCCTTACCTGGTTGAT
<i>18S</i> Reverse Primer	GAGCGACCAAAGGAACCATA
Mouse <i>Il12b</i> Forward Primer	TGGTTTGCCATCGTTTTGCTG
Mouse <i>Il12b</i> Reverse Primer	ACAGGTGAGGTTCACTGTTTCT
Mouse <i>Vcam1</i> Forward Primer	TCTTGGGAGCCTCAACGGTA
Mouse <i>Vcam1</i> Reverse Primer	CAAGTGAGGGCCATGGAGTC
Human <i>Vcam1</i> Forward Primer	GGGAAGATGGTCGTGATCCTT
Human <i>Vcam1</i> Reverse Primer	TCTGGGGTGGTCTCGATTTTA
Mouse <i>Il1b</i> Forward Primer	GCAACTGTTCTGAACTCAACT
Mouse <i>Il1b</i> Reverse Primer	ATCTTTTGGGGTCCGTCAACT
Mouse <i>Colla1</i> Forward Primer	GCTCCTCTTAGGGGCCACT
Mouse <i>Colla1</i> Reverse Primer	CCACGTCTCACCATTGGGG
Mouse <i>Acta2</i> (α SMA) Forward Primer	GTCCCAGACATCAGGGAGTAA
Mouse <i>Acta2</i> (α SMA) Reverse Primer	TCCGATACTTCAGCGTCAGGA
Mouse <i>Pdgfra</i> Forward Primer	ACTACATCTCAAAGGCAGCACCT
Mouse <i>Pdgfra</i> Reverse Primer	TGTAGAACTGGTCGTTCATGGGCA

Supplementary References:

1. Hirsova P, Ibrahim SH, Bronk SF, Yagita H, Gores GJ. Vismodegib suppresses TRAIL-mediated liver injury in a mouse model of nonalcoholic steatohepatitis. *PLoS One*. 2013;8(7):e70599.
2. Fukushima M, Dasgupta D, Mauer AS, Kakazu E, Nakao K, Malhi H. StAR-related lipid transfer domain 11 (STARD11)-mediated ceramide transport mediates extracellular vesicle biogenesis. *The Journal of biological chemistry*. 2018;293(39):15277-89.
3. Ibrahim SH, Hirsova P, Tomita K, Bronk SF, Werneburg NW, Harrison SA, et al. Mixed lineage kinase 3 mediates release of C-X-C motif ligand 10-bearing chemotactic extracellular vesicles from lipotoxic hepatocytes. *Hepatology (Baltimore, Md)*. 2016;63(3):731-44.
4. Brancho D, Ventura JJ, Jaeschke A, Doran B, Flavell RA, Davis RJ. Role of MLK3 in the regulation of mitogen-activated protein kinase signaling cascades. *Molecular and cellular biology*. 2005;25(9):3670-81.
5. Krishnan A, Abdullah TS, Mounajjed T, Hartono S, McConico A, White T, et al. A longitudinal study of whole body, tissue, and cellular physiology in a mouse model of fibrosing NASH with high fidelity to the human condition. *Am J Physiol Gastrointest Liver Physiol*. 2017;312(6):G666-g80.
6. Guo Q, Furuta K, Lucien F, Gutierrez Sanchez LH, Hirsova P, Krishnan A, et al. Integrin beta1-enriched extracellular vesicles mediate monocyte adhesion and promote liver inflammation in murine NASH. *Journal of hepatology*. 2019;71(6):1193-205.
7. Zhao P, Sun X, Chaggan C, Liao Z, In Wong K, He F, et al. An AMPK-caspase-6 axis controls liver damage in nonalcoholic steatohepatitis. *Science (New York, NY)*. 2020;367(6478):652-60.
8. Matsumoto M, Hada N, Sakamaki Y, Uno A, Shiga T, Tanaka C, et al. An improved mouse model that rapidly develops fibrosis in non-alcoholic steatohepatitis. *International journal of experimental pathology*. 2013;94(2):93-103.
9. LeBrasseur NK, Schelhorn TM, Bernardo BL, Cosgrove PG, Loria PM, Brown TA. Myostatin inhibition enhances the effects of exercise on performance and metabolic outcomes in aged mice. *J Gerontol A Biol Sci Med Sci*. 2009;64(9):940-8.
10. Murakami N, Ohtsubo T, Kansui Y, Goto K, Noguchi H, Haga Y, et al. Mice heterozygous for the xanthine oxidoreductase gene facilitate lipid accumulation in adipocytes. *Arteriosclerosis, thrombosis, and vascular biology*. 2014;34(1):44-51.
11. Gutierrez Sanchez LH, Tomita K, Guo Q, Furuta K, Alhuwaish H, Hirsova P, et al. Perinatal Nutritional Reprogramming of the Epigenome Promotes Subsequent

Development of Nonalcoholic Steatohepatitis. *Hepato Comm.* 2018;2(12):1493-512.

12. Kleiner DE, Brunt EM, Van Natta M, Behling C, Contos MJ, Cummings OW, et al. Design and validation of a histological scoring system for nonalcoholic fatty liver disease. *Hepatology (Baltimore, Md)*. 2005;41(6):1313-21.

Supplementary Figure Legends:

Supplementary Fig. 1. Distribution of the differential open chromatin regions in LSEC under lipotoxic treatment. Pie chart showing the genomic distribution of the differentially accessible regions shown in Figure 2B. The promoter region is defined as the sequence of 1 kb upstream to 0.1 kb downstream of a transcription start site (TSS).

UTR: untranslated region.

Supplementary Fig. 2. Lipotoxic stress upregulates VCAM-1 expression in LSEC, via an MLK3-dependent mechanism. (A) Primary human LSEC were treated with vehicle (Veh) or 500 μ M palmitate (PA) for 16 hours, cell viability was assessed using Cell Titer-Glo luminescent assay. (B) TSEC were treated with 500 μ M of PA. Protein levels of VCAM-1 and phosphorylated and total MKK3/6, p38, and JNK were assessed by Western blot. GAPDH was used as a loading control. (C) TSEC were treated with 500 μ M of PA \pm the MLK3 inhibitor URMC-099 (URMC) or 10 μ M of p38 inhibitor SB203580 (SB), or 40 μ M of the JNK inhibitor SP600125. The mRNA expression levels of *Vcam1* were evaluated by real-time qPCR. Fold change was determined after normalization to *18S* rRNA expression, and expressed as fold change to that observed in vehicle (Veh)-treated cells. Graphs present mean \pm SEM, * p <0.05, **** p <0.0001, ns, nonsignificant (unpaired *t*-test, and one-way ANOVA with Bonferroni's multiple

comparison). (D) Eight-week-old wild-type C57BL/6J mice were fed either chow or FFC diet for 24 weeks to induce NASH, and treated with either vehicle (Veh) or 10 mg/kg of the MLK3 inhibitor URM-099 (URMC) twice daily by intraperitoneal injection during the last 2 weeks of the feeding study. Representative images of VCAM-1 immunostaining of liver tissue sections are shown. Scale bar: 100 μ m.

Supplementary Fig. 3. Neither the metabolic phenotype, nor the steatosis was altered by anti-VCAM-1 antibody treatment in FFC-fed mice. Eight-week-old wild-type C57BL/6J mice were fed either chow or FFC diet for 24 weeks to induce NASH, and treated with either anti-VCAM-1 neutralizing antibody (VCAM1Ab) or control IgG isotype antibody (IgG) twice a week for the last 4 weeks. (A) Liver to body weight ratio at the time of sacrifice. (B) Daily caloric intake at 22 weeks of the feeding study. (C) Physical activity, respiratory quotient, and metabolic rate assessed by CLAMS study. (D) Hepatic triglyceride content. (E) HOMA-IR and (F) Glucose tolerance test at 23 weeks of the feeding study (G) Each of the components of the NAS score shown in Figure 4D. (H) Representative images of galectin-3 staining of liver sections (left). Scale bar: 100 μ m. Galectin-3 positive areas were quantified in 10 random 20x microscopic fields and averaged for each animal. n=5-7 per group; Graphs present mean \pm SEM, *p<0.05, **p<0.01, ***p<0.001, ****p<0.0001, ns, nonsignificant (One-way

ANOVA & 2way ANOVA with Bonferroni's multiple comparison).

Supplementary Fig. 4. Intrahepatic leukocyte (IHL) profiling by mass cytometry by time-of-flight (CyTOF). CyTOF was performed on IHL of control IgG-treated chow-fed mice, and FFC-fed mice treated with either VCAM-1 neutralizing antibody or control IgG. Twenty-six unique clusters were defined by a 30 cell surface marker panel (shown in Supplementary Table 5). (A) t-distributed stochastic neighbor embedding (tSNE) plot generated using Rphenograph clustering algorithm (identical to Figure 5A) (B) tSNE plots depicting densities of MHC-I, CD146 and CD45 of cells in each cluster. (C and D) tSNE plots depicting cell surface marker densities of (C) myeloid-lineage cells and Kupffer cells, and (D) lymphocytes of cells in each cluster.

Supplementary Fig. 5. Anti-VCAM1Ab treatment in FFC-fed mice does not significantly alter the granulocyte, dendritic cell, T cell, B cell, and natural killer cell populations. Proportions of cells belonging to specific clusters were quantified for each experimental group. (A) Cluster 13 was categorized into scar-associated macrophages, Cluster 5 into pro-inflammatory monocyte-derived macrophages (MoMF), Cluster 17 into restorative MoMF, (B) Cluster 14 and 20 into Kupffer cells, (C) Cluster 7 into granulocytes, (D) Cluster 10 and 23 into dendritic cells, and (E) Cluster 1, 12, 18, and 24 into T cells, (F) Clusters 6, 11, and 15 into B cells, and (G) Cluster 9 and 25 into

natural killer (NK) cells (n=3 per group); bar graphs represent mean \pm SEM, * $p < 0.05$, ** $p < 0.01$ ***, ns, nonsignificant (One-way ANOVA with Bonferroni's multiple comparison).

Supplementary Fig. 6. AGI-1067 treatment reduced palmitate-induced VCAM-1 expression in TSEC. TSEC were treated with either vehicle (Veh) or 500 μ M of palmitate (PA) \pm AGI-1067 (AGI) for 16 hours. (A) The mRNA expression levels of *Vcam1* were evaluated by real-time qPCR. Fold change was determined after normalization to *18S* rRNA, and expressed as fold change to that observed in vehicle-treated cells. n=3. (B) Protein level of VCAM-1 was assessed by Western blot. Beta-actin was used as a loading control. Primary human LSEC were treated with either Veh or 500 μ M PA \pm AGI or α -tocopherol (TOC) at the indicated μ M concentrations for 16 hours. (C) The mRNA expression levels of *VCAM1* were evaluated by real-time qPCR. n=3. (D) Protein level of VCAM-1 was assessed by Western blot. Beta-actin was used as a loading control. Graphs present mean \pm SEM, **** $p < 0.0001$ (One-way ANOVA with Bonferroni's multiple comparison).

Supplementary Fig. 7. AGI-1067 treatment alters neither the metabolic phenotype nor the steatosis in FFC diet-fed mice. Wild-type C57BL/6J mice were fed either chow or FFC diet for 24 weeks to induce NASH, and treated with 25 mg/kg of AGI-1067 (AGI)

or vehicle daily for the last 2 weeks of the feeding study. (A) Schematic representation of the experimental model. (B) Body weight and liver to body weight ratio at the time of sacrifice. (C) Daily caloric intake. (D) Representative images of H&E staining of liver tissues (scale bar, 100 μ m). Arrows indicate inflammatory cells infiltrate. (E) Hepatic triglyceride content. (F) HOMA-IR at 23 weeks of the feeding study. (G) NAS scores. n=4-5 for each group; Graphs present mean \pm SEM, *p<0.05, **p<0.01, ***p<0.001, ****p<0.0001, ns, nonsignificant (One-way ANOVA with Bonferroni's multiple comparison).

Supplementary Fig. 8. AGI-1067 treatment in FFC-fed mice attenuates hepatic injury, inflammation and fibrosis. Wild-type C57BL/6J mice were fed either chow or FFC diet for 24 weeks to induce NASH, and treated with or without 25 mg/kg of AGI-1067 (AGI) or vehicle daily for the last 2 weeks of the feeding study. (A) Quantification of TUNEL-positive cells. (B) Plasma ALT levels. (C) Representative images of F4/80 staining of liver sections. (D) Hepatic mRNA expression levels of *Cd68*, *Il1b*, and *Tnf* were assessed by real-time PCR. Fold change was determined after normalization to *18S* rRNA and expressed relative to chow-fed mice. (E) Representative images of Sirius red staining, quantification of Sirius red-positive areas. (F) Representative images of α -SMA staining of liver sections, quantification of α -SMA-positive areas. (G) Hepatic

mRNA expressions of *Collagen1a1* and *Acta2* (α -SMA) assessed by real-time PCR. Fold change was determined after normalization to *18S* rRNA and expressed relative to chow-fed mice. Scale bars: 100 μ m; n=4-5 for each group; Graphs present mean \pm SEM, *p<0.05, **p<0.01, ***p<0.001, ****p<0.0001, ns, nonsignificant (One-way ANOVA with Bonferroni's multiple comparison).

Supplementary Fig. 9. CD-HFD can rapidly induce murine NASH with significant steatosis, inflammation, and fibrosis. Wild-type C57BL/6J mice at the age of 8 weeks were fed CD-HFD diet for 4, 6, or 8 weeks to induce NASH. Biochemical, histological, and mRNA expression of CD-HFD-fed mice were compared with 24 weeks chow- or FFC-fed mice. (A) Body weight curves during the feeding study and liver-to-body weight ratios. (B) Plasma ALT levels. (C) Hepatic mRNA expression levels of *Vcam1* were assessed by real-time PCR. Fold change was determined after normalization to *18S* rRNA and expressed relative to chow-fed mice. (D) Representative images of H&E staining of liver tissues (scale bar, 100 μ m). (E) Hepatic mRNA expression levels of *Ccr2*, *Tnf*, *Colla1*, and *Acta2* were assessed by real-time PCR. Fold change was determined after normalization to *18S* rRNA and expressed relative to chow-fed mice. (F) Representative images of Sirius red staining of liver tissues (scale bar, 100 μ m), quantification of Sirius red-positive areas. n=4-5 per group; Graphs present mean \pm

SEM, * $p < 0.05$, ** $p < 0.01$, *** $p < 0.001$, **** $p < 0.0001$ (One-way ANOVA with Bonferroni's multiple comparison).

Supplementary Fig. 10. Vcam1^{Δend} mice show efficient Vcam1 deletion in LSEC and

unaltered metabolic phenotype when fed a CD-HFD NASH-inducing diet. (A) The

mRNA expression levels of *Vcam1* in LSEC isolated from *Vcam1^{fl/fl}* and *Vcam1^{Δend}*

mice fed the chow diet were examined by real-time PCR at the age of 14 weeks. Fold

change was determined after normalization to *18S* rRNA and expressed relative to

Vcam1^{fl/fl} mice. (B-F) *Vcam1^{fl/fl}* and *Vcam1^{Δend}* mice were fed the CD-HFD diet starting

at the age of 8 weeks for 6 weeks to induce NASH. (B) Western blots showing the

expressions of VCAM-1 in non-parenchymal hepatic cells other than LSEC from

CD-HFD-fed *Vcam1^{fl/fl}* and *Vcam1^{Δend}* mice. Beta-actin was used as a loading control

(the dotted line indicates excluded mouse due to poor protein quality) (left).

Quantification of VCAM-1 protein level relative to β -actin was assessed by

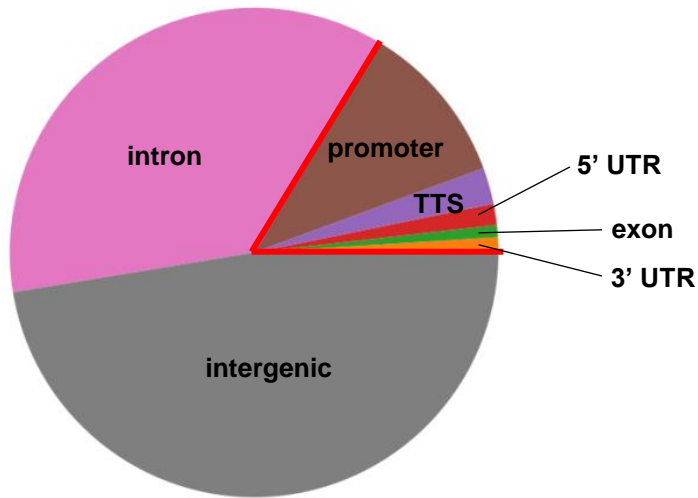
densitometry (right). (C) Body weight (D) Liver-to-body weight ratios at the time of

sacrifice. (E) Hepatic triglyceride content. (F) Separate analysis of the components of

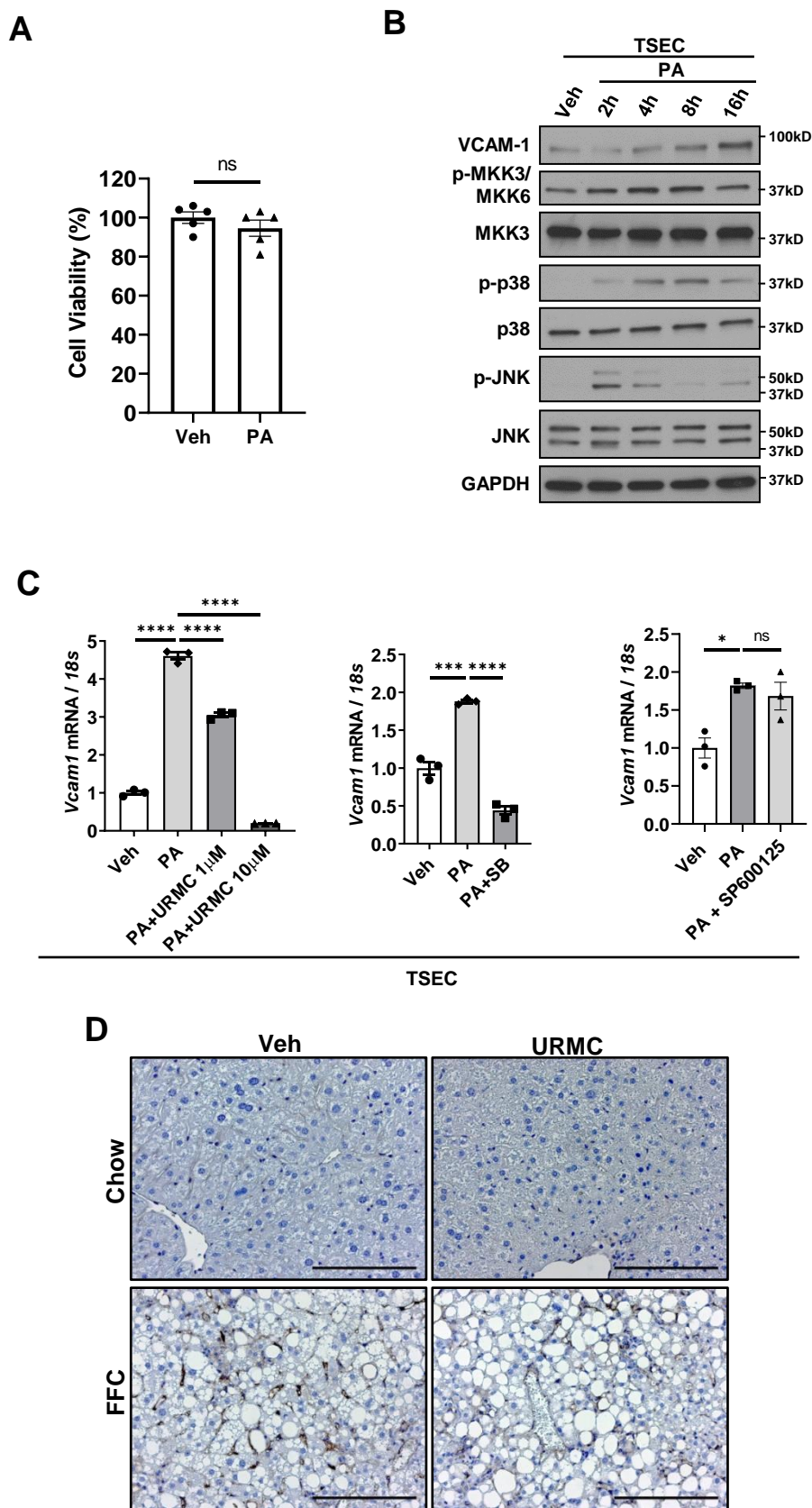
the NAS score shown in Figure 7E. Graphs present mean \pm SEM, ** $p < 0.01$,

**** $p < 0.0001$, ns, nonsignificant (Unpaired *t*-test).

Supplementary Figure 1

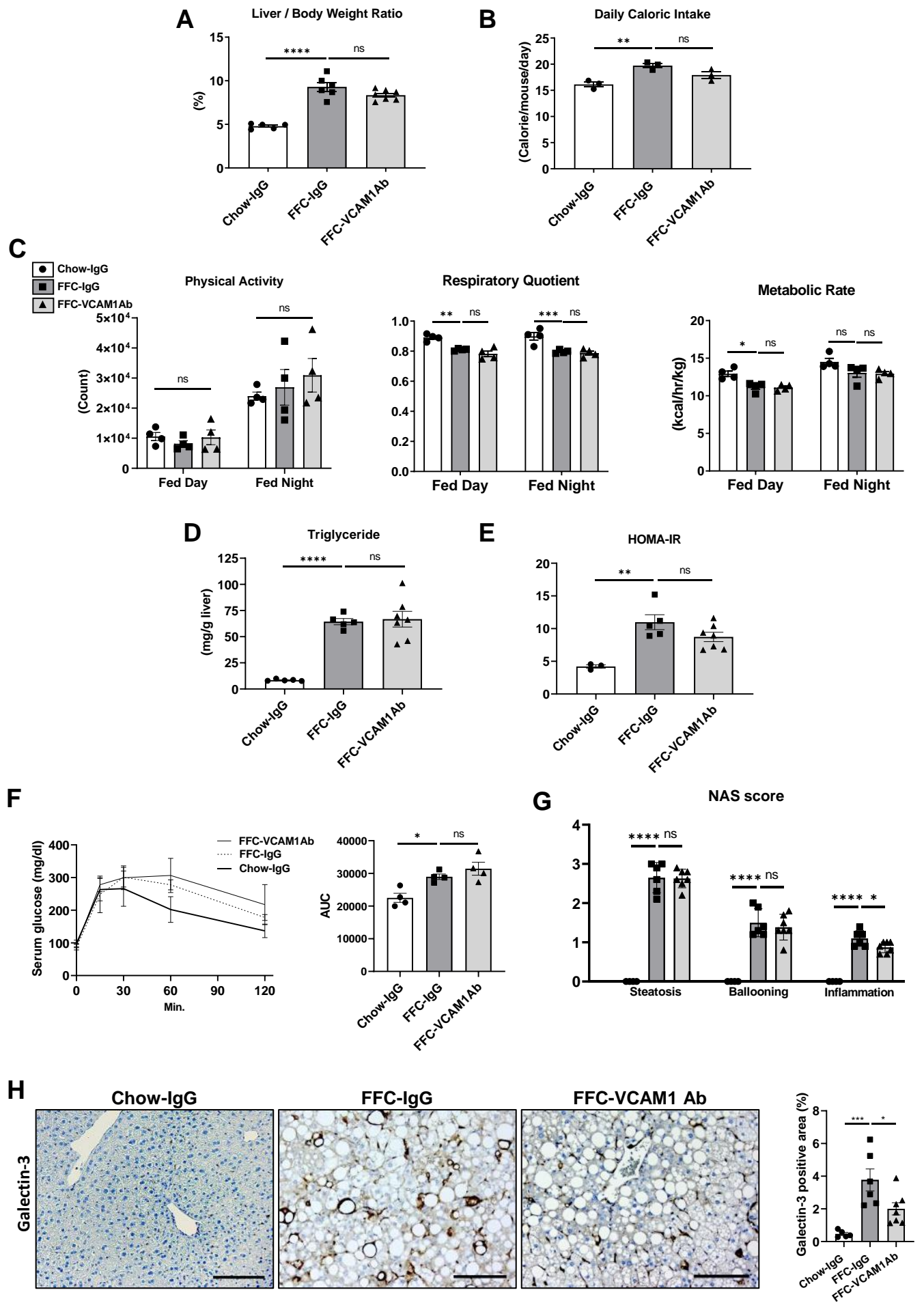


Supplementary Fig. 1. Distribution of the differential open chromatin regions in LSEC under lipotoxic treatment. Pie chart showing the genomic distribution of the differentially accessible regions shown in Figure 2B. The promoter region is defined as the sequence of 1 kb upstream to 0.1 kb downstream of a transcription start site (TSS). UTR: untranslated region.



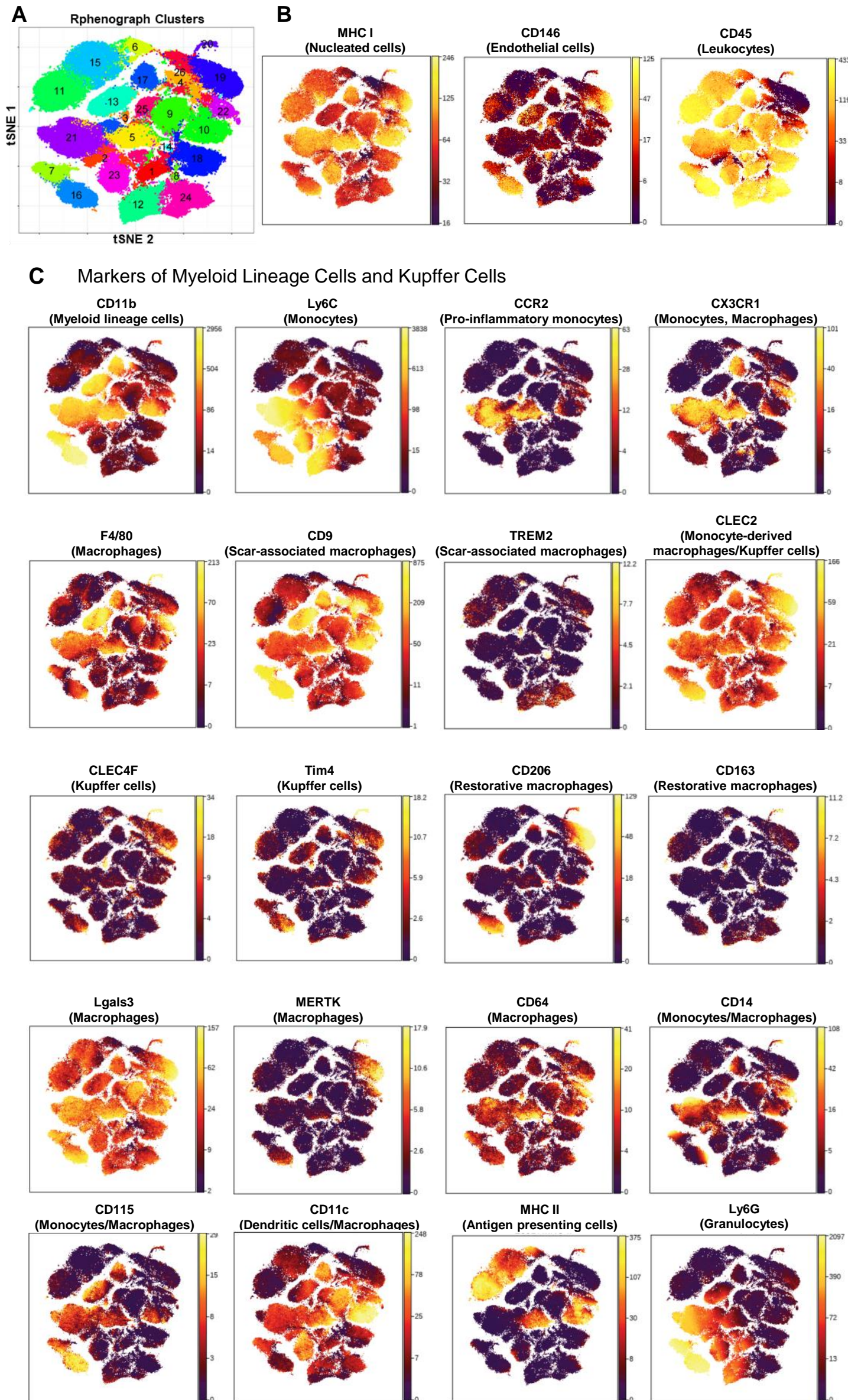
Supplementary Fig. 2. Lipotoxic stress upregulates VCAM-1 expression in LSEC, via an MLK3-dependent mechanism. (A) Primary human LSEC were treated with vehicle (Veh) or 500 μ M palmitate (PA) for 16 hours, cell viability was assessed using Cell Titer-Glo luminescent assay. (B) TSEC were treated with 500 μ M of PA. Protein levels of VCAM-1 and phosphorylated and total MKK3/6, p38, and JNK were assessed by Western blot. GAPDH was used as a loading control. (C) TSEC were treated with 500 μ M of PA \pm the MLK3 inhibitor URMC-099 (URMC) or 10 μ M of p38 inhibitor SB203580 (SB), or 40 μ M of the JNK inhibitor SP600125. The mRNA expression levels of *Vcam1* were evaluated by real-time qPCR. Fold change was determined after normalization to *18S* rRNA expression, and expressed as fold change to that observed in vehicle (Veh)-treated cells. Graphs present mean \pm SEM, * p <0.05, **** p <0.0001, ns, nonsignificant (unpaired t -test, and one-way ANOVA with Bonferroni's multiple comparison). (D) Eight-week-old wild-type C57BL/6J mice were fed either chow or FFC diet for 24 weeks to induce NASH, and treated with either vehicle (Veh) or 10 mg/kg of the MLK3 inhibitor URMC-099 (URMC) twice daily by intraperitoneal injection during the last 2 weeks of the feeding study. Representative images of VCAM-1 immunostaining of liver tissue sections are shown. Scale bar: 100 μ m.

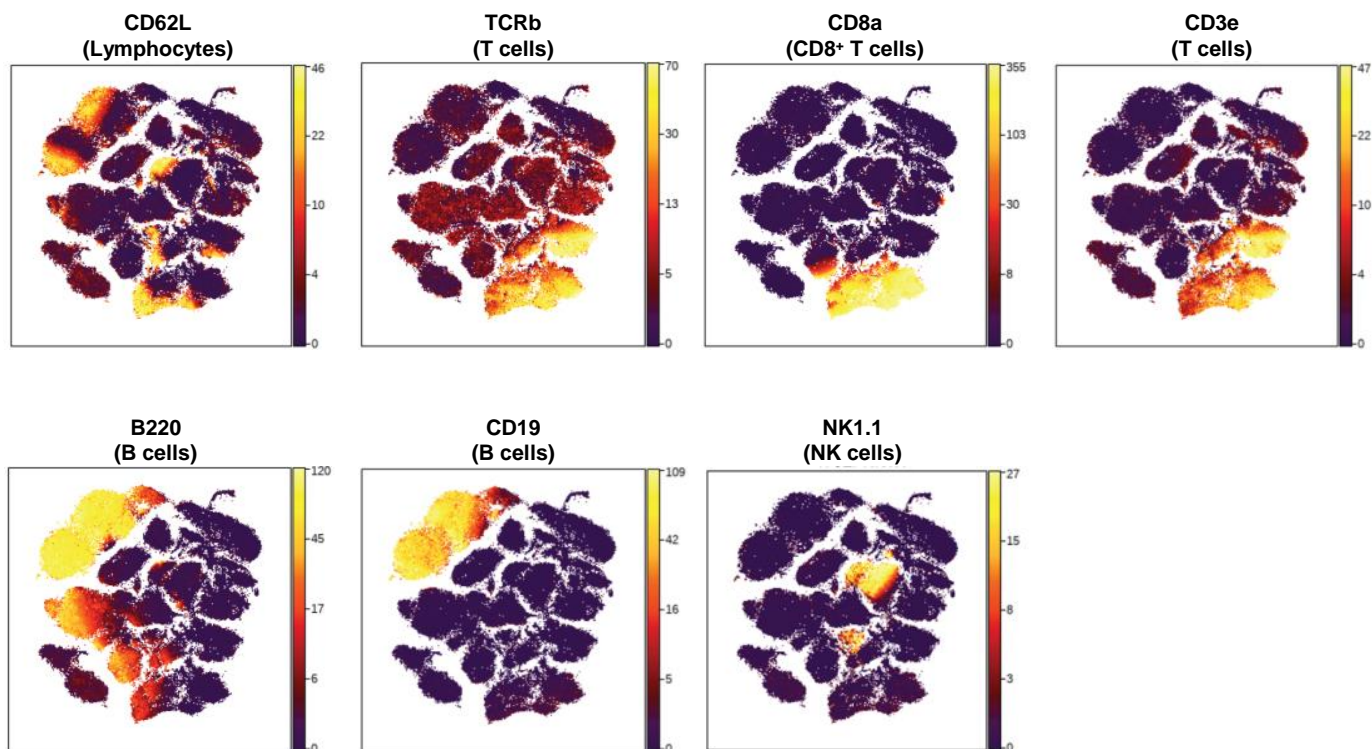
Supplementary Figure 3



Supplementary Fig. 3. Neither the metabolic phenotype, nor the steatosis was altered by anti-VCAM-1 antibody treatment in FFC-fed mice. Eight-week-old wild-type C57BL/6J mice were fed either chow or FFC diet for 24 weeks to induce NASH, and treated with either anti-VCAM-1 neutralizing antibody (VCAM1Ab) or control IgG isotype antibody (IgG) twice a week for the last 4 weeks. (A) Liver to body weight ratio at the time of sacrifice. (B) Daily caloric intake at 22 weeks of the feeding study. (C) Physical activity, respiratory quotient, and metabolic rate assessed by CLAMS study. (D) Hepatic triglyceride content. (E) HOMA-IR and (F) Glucose tolerance test at 23 weeks of the feeding study (G) Each of the components of the NAS score shown in Figure 4D. (H) Representative images of galectin-3 staining of liver sections (left). Scale bar: 100 μm. Galectin-3 positive areas were quantified in 10 random 20x microscopic fields and averaged for each animal. n=5-7 per group; Graphs present mean ± SEM, *p<0.05, **p<0.01, ***p<0.001, ****p<0.0001, ns, nonsignificant (One-way ANOVA & 2way ANOVA with Bonferroni's multiple comparison).

Supplementary Figure 4

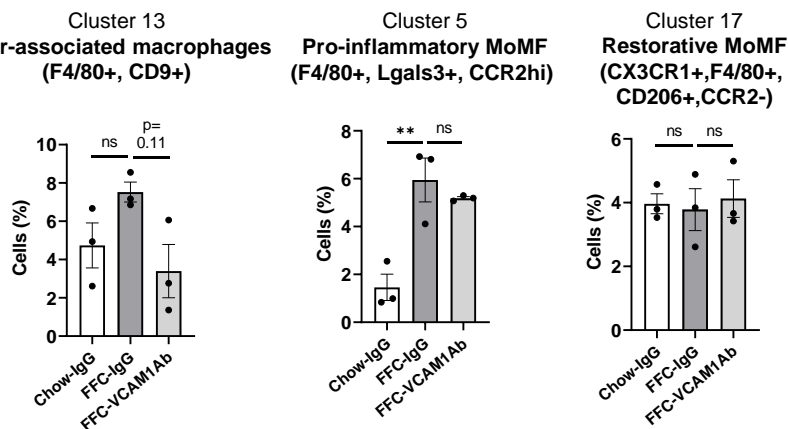


D Markers of Lymphocytes**Supplementary Fig. 4. Intrahepatic leukocyte (IHL) profiling by mass cytometry by time-of-flight (CyTOF).**

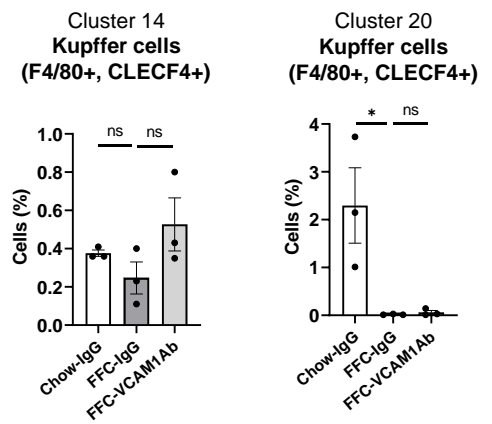
CyTOF was performed on IHL of control IgG-treated chow-fed mice, and FFC-fed mice treated with either VCAM-1 neutralizing antibody or control IgG. Twenty-six unique clusters were defined by a 30 cell surface marker panel (shown in Supplementary Table 5). (A) t-distributed stochastic neighbor embedding (tSNE) plot generated using Rphenograph clustering algorithm (identical to Figure 5A) (B) tSNE plots depicting densities of MHC-I, CD146 and CD45 of cells in each cluster. (C and D) tSNE plots depicting cell surface marker densities of (C) myeloid-lineage cells and Kupffer cells, and (D) lymphocytes of cells in each cluster.

Supplementary Figure 5

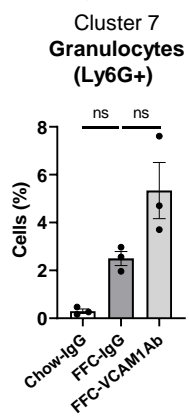
A



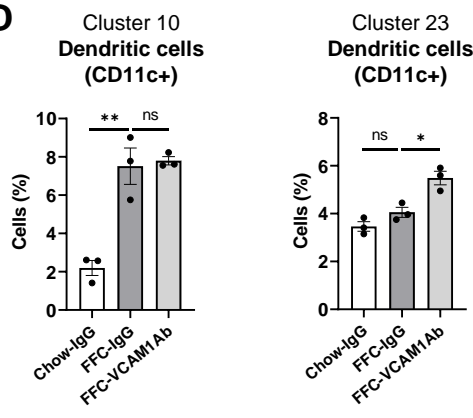
B



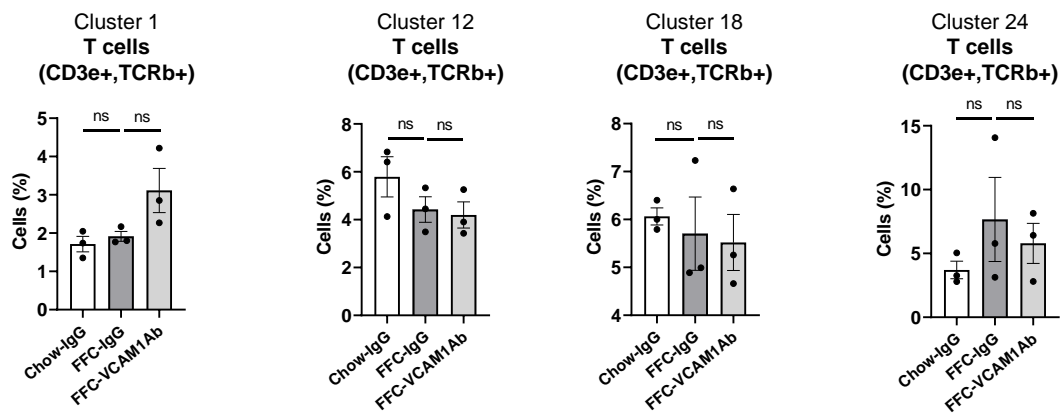
C



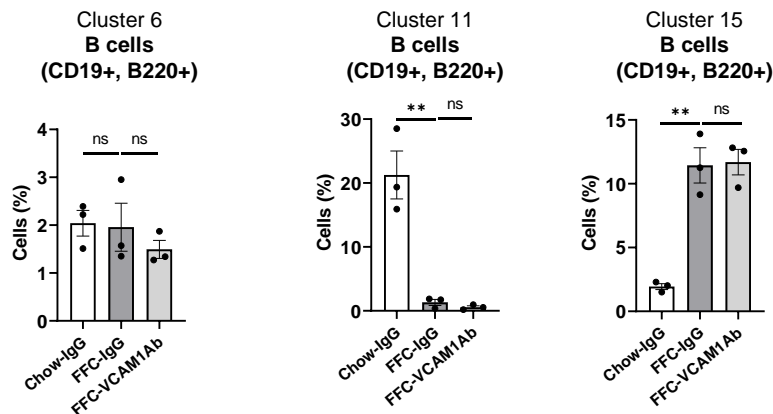
D



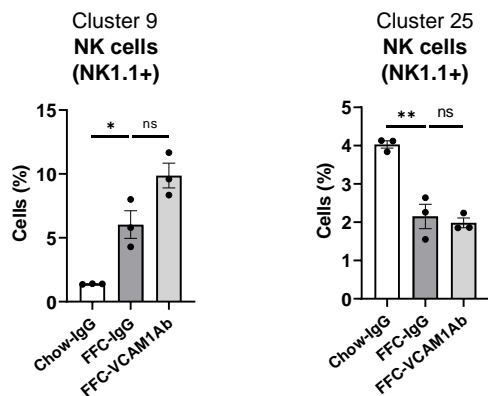
E



F

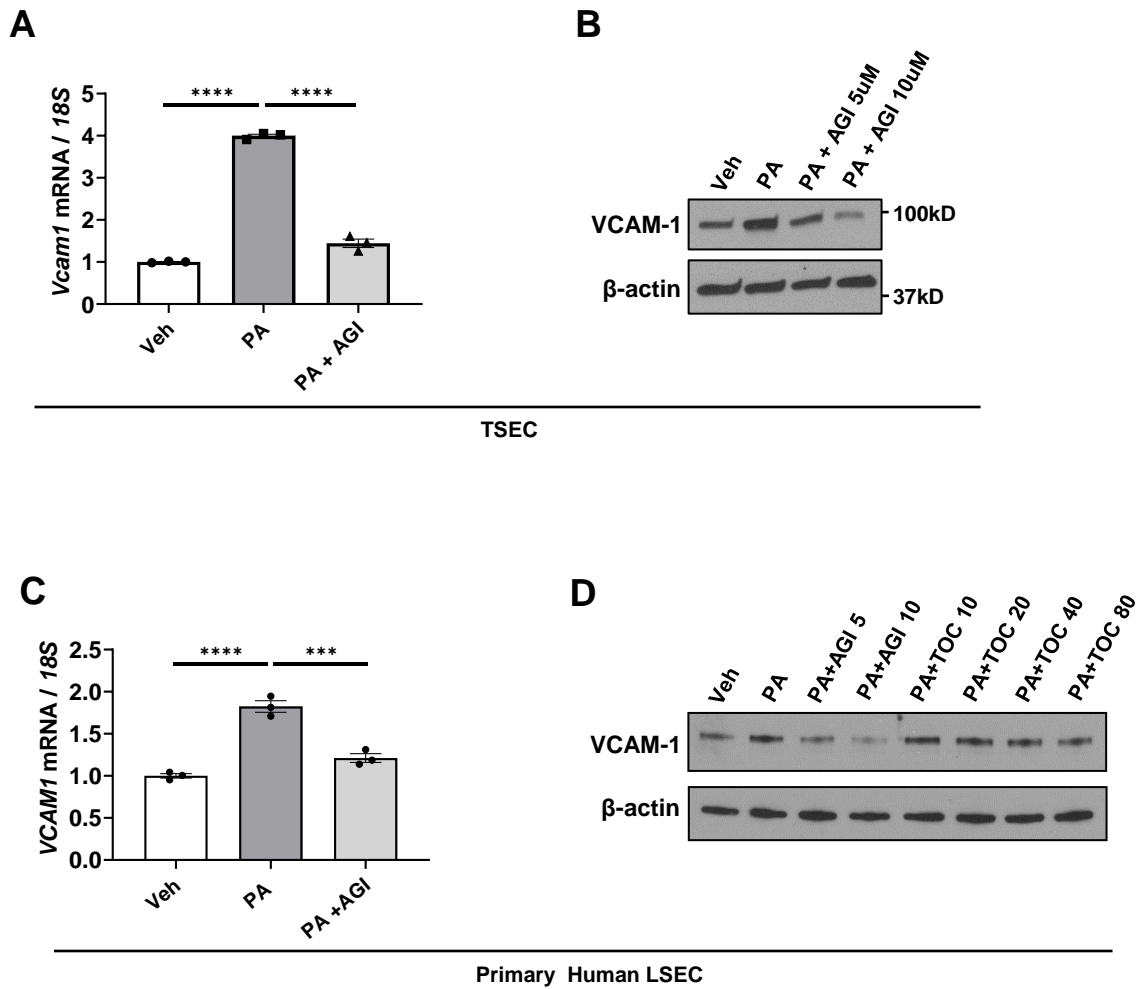


G



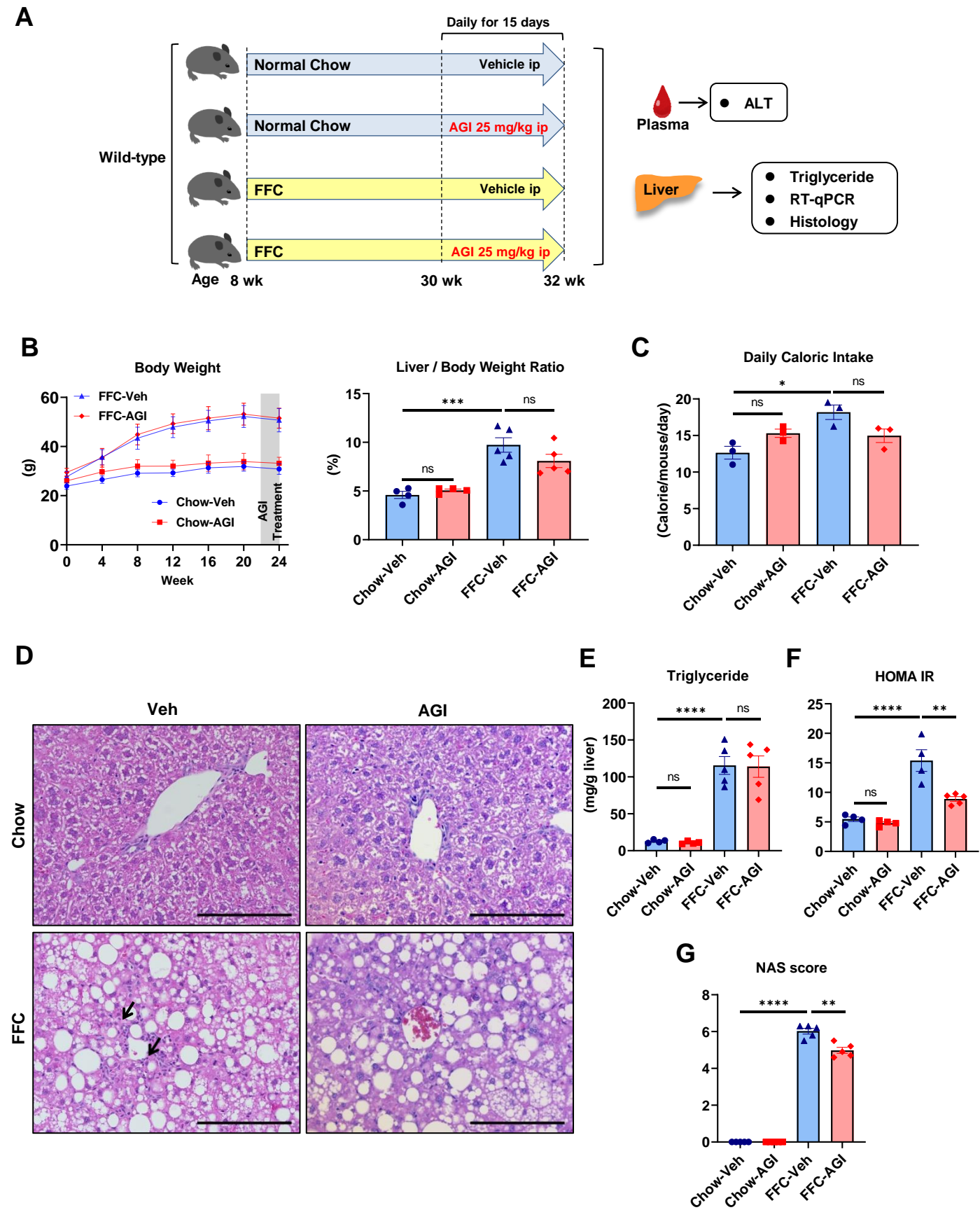
Supplementary Fig. 5. Anti-VCAM1Ab treatment in FFC-fed mice does not significantly alter the granulocyte, dendritic cell, T cell, B cell, and natural killer cell populations. Proportions of cells belonging to specific clusters were quantified for each experimental group. (A) Cluster 13 was categorized into scar-associated macrophages, Cluster 5 into pro-inflammatory monocyte-derived macrophages (MoMF), Cluster 17 into restorative MoMF, (B) Cluster 14 and 20 into Kupffer cells, (C) Cluster 7 into granulocytes, (D) Cluster 10 and 23 into dendritic cells, and (E) Cluster 1, 12, 18, and 24 into T cells, (F) Clusters 6, 11, and 15 into B cells, and (G) Cluster 9 and 25 into natural killer (NK) cells (n=3 per group); bar graphs represent mean \pm SEM, *p < 0.05, **p < 0.01, ***p < 0.001, ns, nonsignificant (One-way ANOVA with Bonferroni's multiple comparison).

Supplementary Figure 6



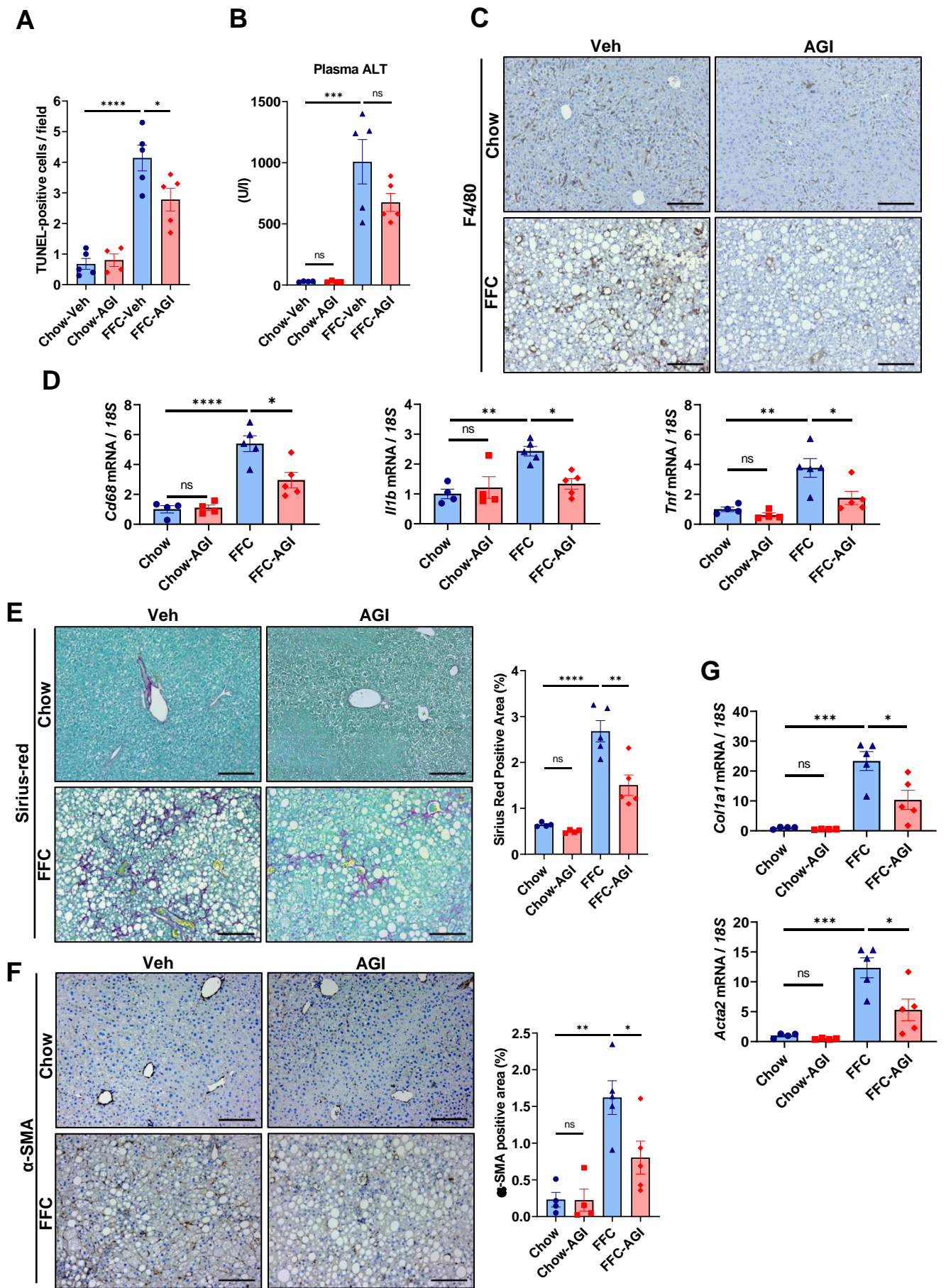
Supplementary Fig. 6. AGI-1067 treatment reduced palmitate-induced VCAM-1 expression in TSEC. TSEC were treated with either vehicle (Veh) or 500 μ M of palmitate (PA) \pm AGI-1067 (AGI) for 16 hours. (A) The mRNA expression levels of *Vcam1* were evaluated by real-time qPCR. Fold change was determined after normalization to *18S* rRNA, and expressed as fold change to that observed in vehicle-treated cells. n=3. (B) Protein level of VCAM-1 was assessed by Western blot. Beta-actin was used as a loading control. Primary human LSEC were treated with either Veh or 500 μ M PA \pm AGI or α -tocopherol (TOC) at the indicated μ M concentrations for 16 hours. (C) The mRNA expression levels of *VCAM1* were evaluated by real-time qPCR. n=3. (D) Protein level of VCAM-1 was assessed by Western blot. Beta-actin was used as a loading control. Graphs present mean \pm SEM, ****p<0.0001 (One-way ANOVA with Bonferroni's multiple comparison).

Supplementary Figure 7



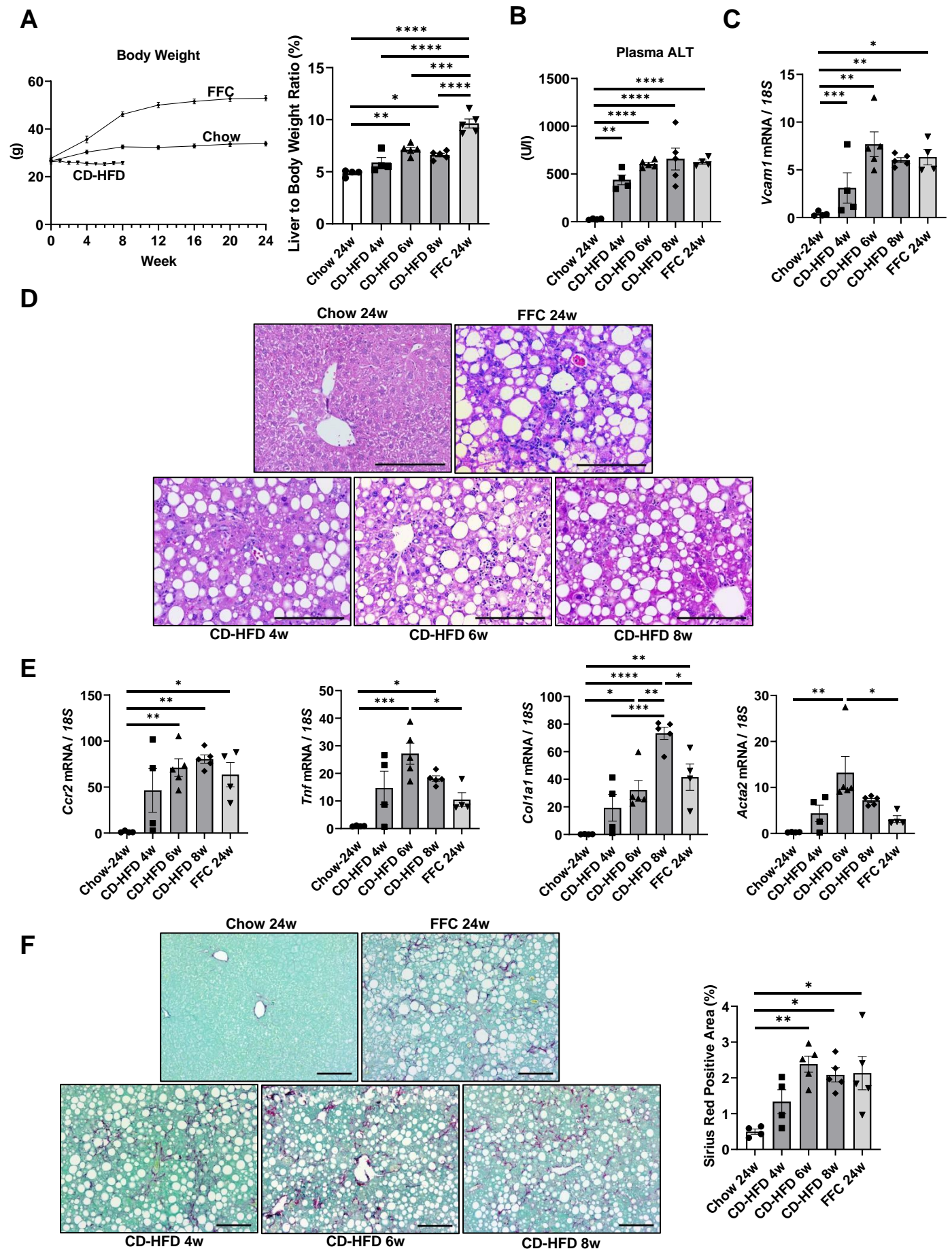
Supplementary Fig. 7. AGI-1067 treatment alters neither the metabolic phenotype nor the steatosis in FFC diet-fed mice. Wild-type C57BL/6J mice were fed either chow or FFC diet for 24 weeks to induce NASH, and treated with 25 mg/kg of AGI-1067 (AGI) or vehicle daily for the last 2 weeks of the feeding study. (A) Schematic representation of the experimental model. (B) Body weight and liver to body weight ratio at the time of sacrifice. (C) Daily caloric intake. (D) Representative images of H&E staining of liver tissues (scale bar, 100 μ m). Arrows indicate inflammatory cells infiltrate. (E) Hepatic triglyceride content. (F) HOMA-IR at 23 weeks of the feeding study. (G) NAS scores. n=4-5 for each group; Graphs present mean \pm SEM, * p <0.05, ** p <0.01, *** p <0.001, **** p <0.0001, ns, nonsignificant (One-way ANOVA with Bonferroni's multiple comparison).

Supplementary Figure 8

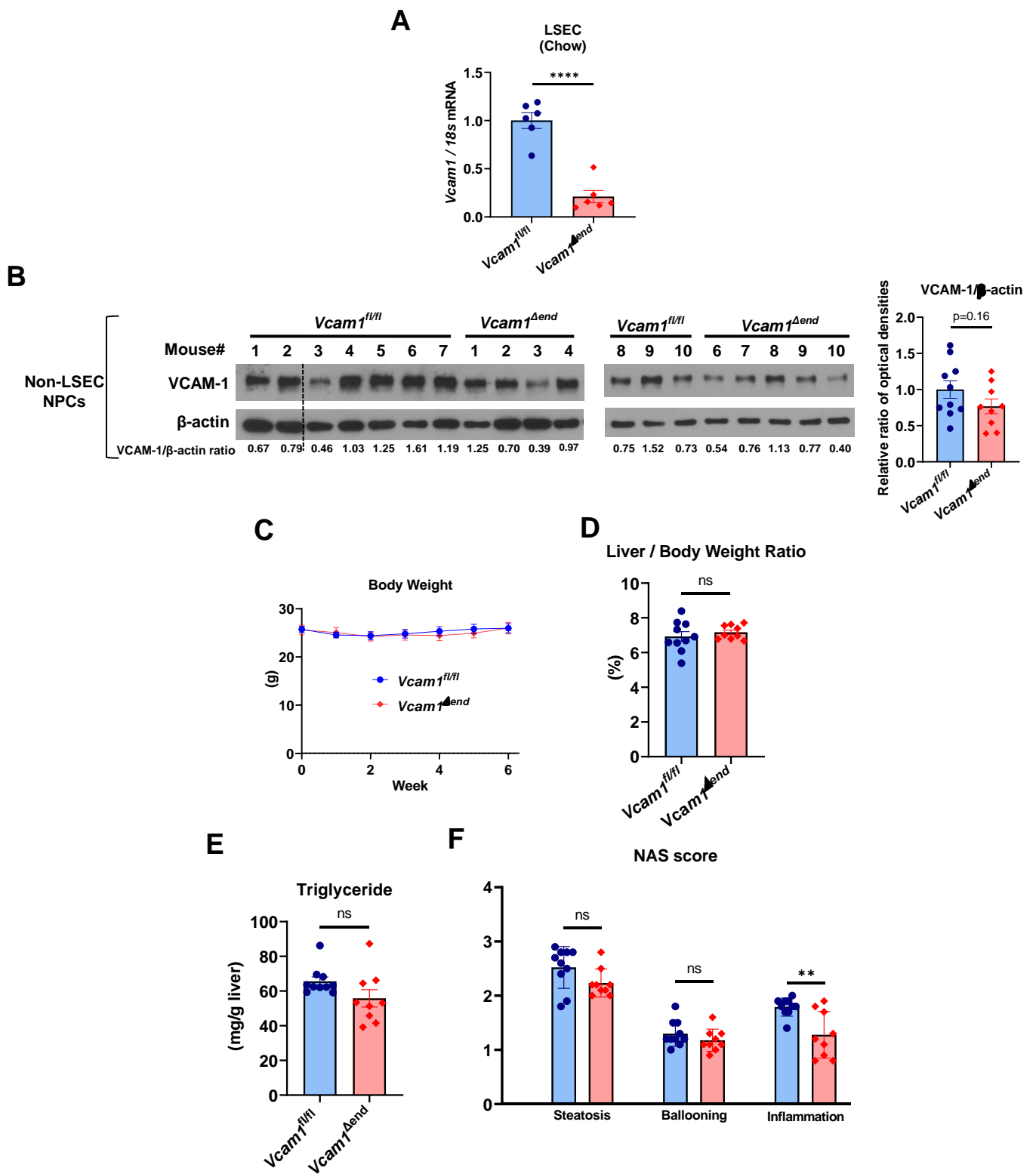


Supplementary Fig. 8. AGI-1067 treatment in FFC-fed mice attenuates hepatic injury, inflammation and fibrosis. Wild-type C57BL/6J mice were fed either chow or FFC diet for 24 weeks to induce NASH, and treated with or without 25 mg/kg of AGI-1067 (AGI) or vehicle daily for the last 2 weeks of the feeding study. (A) Quantification of TUNEL-positive cells. (B) Plasma ALT levels. (C) Representative images of F4/80 staining of liver sections. (D) Hepatic mRNA expression levels of *Cd68*, *Il1b*, and *Tnf* were assessed by real-time PCR. Fold change was determined after normalization to *18S* rRNA and expressed relative to chow-fed mice. (E) Representative images of Sirius red staining, quantification of Sirius red-positive areas. (F) Representative images of α -SMA staining of liver sections, quantification of α -SMA-positive areas. (G) Hepatic mRNA expressions of *Collagen1a1* and *Acta2* (α -SMA) assessed by real-time PCR. Fold change was determined after normalization to *18S* rRNA and expressed relative to chow-fed mice. Scale bars: 100 μ m; n=4-5 for each group; Graphs present mean \pm SEM, * p <0.05, ** p <0.01, *** p <0.001, **** p <0.0001, ns, nonsignificant (One-way ANOVA with Bonferroni's multiple comparison).

Supplementary Figure 9



Supplementary Fig. 9. CD-HFD can rapidly induce murine NASH with significant steatosis, inflammation, and fibrosis. Wild-type C57BL/6J mice at the age of 8 weeks were fed CD-HFD diet for 4, 6, or 8 weeks to induce NASH. Biochemical, histological, and mRNA expression of CD-HFD-fed mice were compared with 24 weeks chow- or FFC-fed mice. (A) Body weight curves during the feeding study and liver-to-body weight ratios. (B) Plasma ALT levels. (C) Hepatic mRNA expression levels of *Vcam1* were assessed by real-time PCR. Fold change was determined after normalization to *18S* rRNA and expressed relative to chow-fed mice. (D) Representative images of H&E staining of liver tissues (scale bar, 100 μ m). (E) Hepatic mRNA expression levels of *Ccr2*, *Tnf*, *Col1a1*, and *Acta2* were assessed by real-time PCR. Fold change was determined after normalization to *18S* rRNA and expressed relative to chow-fed mice. (F) Representative images of Sirius red staining of liver tissues (scale bar, 100 μ m), quantification of Sirius red-positive areas. $n=4-5$ per group; Graphs present mean \pm SEM, * $p<0.05$, ** $p<0.01$, *** $p<0.001$, **** $p<0.0001$ (One-way ANOVA with Bonferroni's multiple comparison).



Supplementary Fig. 10. *Vcam1*^{Δend} mice show efficient *Vcam1* deletion in LSEC and unaltered metabolic phenotype when fed a CD-HFD NASH-inducing diet. (A) The mRNA expression levels of *Vcam1* in LSEC isolated from *Vcam1*^{fl/fl} and *Vcam1*^{Δend} mice fed the chow diet were examined by real-time PCR at the age of 14 weeks. Fold change was determined after normalization to 18S rRNA and expressed relative to *Vcam1*^{fl/fl} mice. (B-F) *Vcam1*^{fl/fl} and *Vcam1*^{Δend} mice were fed the CD-HFD diet starting at the age of 8 weeks for 6 weeks to induce NASH. (B) Western blots showing the expressions of VCAM-1 in non-parenchymal hepatic cells other than LSEC from CD-HFD-fed *Vcam1*^{fl/fl} and *Vcam1*^{Δend} mice. Beta-actin was used as a loading control (the dotted line indicates excluded mouse due to poor protein quality) (left). Quantification of VCAM-1 protein level relative to β-actin was assessed by densitometry (right). (C) Body weight (D) Liver-to-body weight ratios at the time of sacrifice. (E) Hepatic triglyceride content. (F) Separate analysis of the components of the NAS score shown in Figure 7E. Graphs present mean ± SEM, **p<0.01, ****p<0.0001, ns, nonsignificant (Unpaired *t*-test).